Limnol. Oceanogr., 56(6), 2011, 2293–2307
© 2011, by the Association for the Sciences of Limnology and Oceanography, Inc.
doi:10.4319/lo.2011.56.6.2293

Shutdown of turbulent convection as a new criterion for the onset of spring phytoplankton blooms

John R. Taylor[a] and Raffaele Ferrari[b,*]

[a] Department of Applied Mathematics and Theoretical Physics, University of Cambridge, Cambridge, UK
[b] Department of Earth, Atmospheric and Planetary Sciences, Massachusetts Institute of Technology, Cambridge, Massachusetts

Abstract

The onset of phytoplankton blooms in late winter, early spring has been traditionally associated with the shoaling of the mixed layer above a critical depth. Here we show that the onset of a bloom can also be triggered by a reduction in air–sea fluxes at the end of winter. When net cooling subsides at the end of winter, turbulent mixing becomes weak, thereby increasing the residence time of phytoplankton cells in the euphotic layer and allowing a bloom to develop. The necessary change in the air–sea flux generally precedes mixed-layer shoaling, and may provide a better indicator for the onset of the spring bloom than the mixed-layer depth alone. Our hypothesis is supported by numerical simulations and remote sensing data.

The annual cycle of phytoplankton growth in many parts of the ocean is dominated by a dramatic population increase known as the spring bloom. High levels of primary production during the spring bloom, and the subsequent sinking of organic material, contribute significantly to the carbon flux to the deep ocean (Smetacek et al. 1978; Townsend et al. 1994). The spring bloom occurs globally in coastal seas, lakes, in the Mediterranean and Black Seas, and most famously in the North Atlantic, where the associated change in ocean color can be seen from space. Although it has been the focus of research for decades, there is an ongoing debate as to what conditions prompt the onset of the spring bloom (Townsend et al. 1994; Huisman et al. 1999; Behrenfeld 2010).

The onset of phytoplankton blooms is affected by many factors including turbulent mixing and light exposure (the physical controls), respiration and predation rates (the biological controls), and the availability of essential nutrients (the chemical controls) as described for example in Miller (2004). Here, we focus on identifying the most important physical controls. The depth of the *mixed layer*, where density is nearly homogeneous in the vertical, has been traditionally identified as the crucial physical control for the onset of blooms. According to the 'critical depth' hypothesis (Gran and Braarud 1935; Riley 1946; Sverdrup 1953), strong wind and buoyancy forcing during winter lead to deep mixed layers, rich in nutrients entrained from the underlying thermocline. However, at this time the mixed layer is typically deeper than a critical depth, H_C, and primary production is limited by light availability despite the abundance of nutrients. A bloom then develops in spring when the mixed layer becomes shallower than the critical depth and phytoplankton cells are exposed to sufficient light to support net population growth. An expression for the critical depth, H_C, was derived by Sverdrup (1953):

$$H_C \sim h_l \frac{\mu_0}{m} \tag{1}$$

where μ_0 is the local population growth rate at the ocean surface, h_l is the e-folding depth of light penetration, and m is the loss rate.

The critical-depth hypothesis has served as a cornerstone in biological oceanography for decades, but it has been questioned recently, particularly for its ability to predict the onset of the bloom. Several authors have reported the occurrence of phytoplankton blooms in deep mixed layers. Townsend et al. (1992) observed a phytoplankton bloom in the Gulf of Maine at a time when the mixed layer was about a factor of two deeper than the estimated critical depth. Dale and Heimdal (1999) compiled several years of data from Ocean Weather Ship Station Mike (66°N, 2°E) and found that the phytoplankton population starts to increase several weeks before the upper ocean restratifies. More recently, Behrenfeld (2010) and Boss and Behrenfeld (2010) observed growth in the bulk phytoplankton population starting in late autumn or early winter when the mixed layers were still deepening.

In formulating the critical depth hypothesis, Sverdrup (1953) supposed that turbulence in the mixed layer is "strong enough to distribute the plankton organisms evenly through the layer." There are two assumptions associated with this statement: the full mixed layer is actively turbulent, and the strength of turbulent mixing is sufficient to overcome any process leading to an accumulation of cells at a particular depth. A more complete characterization of the problem must include both the depth and intensity of mixing (Huisman et al. 1999). Furthermore, it is important to distinguish between a 'mixed layer' with uniform density and a 'mixing layer' with a uniform density *and* active turbulence (Brainerd and Gregg 1995).

Several previous studies have proposed that weak turbulent mixing can lead to the observed phytoplankton growth in deep mixed layers. Huisman et al. (1999) and Ghosal and Mandre (2003) solved a one-dimensional model for the phytoplankton concentration with a constant turbulent diffusivity. They found that when the mixing layer is deeper than the critical depth, growth in the integrated phytoplankton population is possible if the

* Corresponding author: rferrari@mit.edu

turbulent diffusivity is smaller than a critical threshold. Ebert et al. (2001) extended this work by deriving analytical solutions to a one-dimensional phytoplankton model including sinking, buoyancy, self-shading, and a constant turbulent diffusivity. Huisman et al. (2002) showed that sinking phytoplankton species in a deep mixing layer are able to grow at intermediate turbulence levels where turbulence is strong enough to keep the cells suspended in the water column, but not too strong to prevent growth through light limitation. Huisman et al. (2004) examined the practical implications of the 'critical turbulence' hypothesis in an artificially mixed lake and found that the dominant phytoplankton species with and without mixing were consistent with the model predictions. Peeters et al. (2007) found that the onset of a phytoplankton bloom in Upper Lake Constance closely coincided with a decrease in turbulent mixing at the end of winter.

A common feature of these previous studies is that they characterized the intensity of turbulent mixing using a turbulent diffusivity, κ_T. In nature, the turbulent diffusivity is not an externally prescribed parameter, but rather depends on factors like the atmospheric forcing (e.g., cooling or wind), and the density stratification. One of the primary objectives of this study is to relate the critical turbulent diffusivity to the atmospheric forcing conditions, and to derive a criterion for the onset of the spring bloom in terms of the atmospheric forcing. We are interested in the transition from winter to spring in the open ocean; therefore, we will focus on convectively driven mixing, which is responsible for generating deep wintertime mixed layers at high latitudes. The criterion will then be tested using high-resolution three-dimensional numerical simulations, which resolve most of the convective turbulence. Although our focus will be on thermal convection, our results can be generalized to turbulence driven by wind forcing and evaporation.

A simple thought experiment illustrates how changes in atmospheric forcing can lead to phytoplankton growth. Consider typical winter conditions with deep, nutrient-rich mixed layers. Strong atmospheric forcing continually mixes phytoplankton out of the euphotic layer and prevents growth, in accordance with the critical depth hypothesis. When spring comes and the atmospheric forcing weakens, active turbulence quickly subsides before the mixed-layer shoals. At this point, before stratification develops, growth can start as soon the rate of mixing becomes slower than the net phytoplankton growth near the surface (Huisman et al. 1999).

Our analysis shows that the critical atmospheric forcing required to trigger a bloom is very weak, and for most practical purposes indistinguishable from zero. Hence, our hypothesis is that a bloom can develop when the atmospheric cooling shuts off, regardless of the details of the biological or physical response. This hypothesis is more readily testable than the critical depth or critical turbulence criteria. Calculating the critical depth using the expression in Eq. 1 requires knowledge of the net phytoplankton growth and loss rates, which depend on many factors and are difficult to accurately measure in situ. Evaluating the critical turbulence hypothesis requires a measurement of the turbulent diffusivity, which requires specialized instruments to measure fine-scale velocity or temperature fluctuations. In comparison, the atmospheric forcing is much more readily available based on data collected from research vessels, mooring arrays, weather stations, and by satellite.

The hypothesis that phytoplankton growth can be related to meteorological conditions has support in previous studies. In an early modeling study, Jamart et al. (1977) imposed a decrease in the depth and intensity of mixing in the spring following an increase in solar radiation, and the reduction in mixing triggered a phytoplankton bloom. More recently, Waniek (2003) used a bulk mixed-layer model forced with observed atmospheric fluxes and found that the inter-annual variability in the timing and intensity of the bloom was controlled by changes in the meteorological forcing. Similar conclusions have also been drawn more directly from observations. For example, Dutkiewicz et al. (2001) and Follows and Dutkiewicz (2002) found that in the subpolar North Atlantic, where deep wintertime mixed layers and strong spring bloom events are seen, the mean spring phytoplankton concentration is inversely proportional to the strength of meteorological forcing. Similarly, Henson et al. (2006) found that the timing and intensity of the spring bloom, inferred from satellite observations, is correlated with the intensity of wintertime wind and convective forcing.

The focus of this study is on the period of rapid growth at the onset of the spring bloom, and this focus will influence our modeling approach and assumptions. Specifically, we will assume that nutrients are abundant, the loss rate is constant in time, and phytoplankton growth is proportional to light availability. In focusing on the period of rapid growth, we also assume that changes in the phytoplankton growth and loss rates and the mixed-layer depth are slow compared to the phytoplankton growth rate. As a result, we will not consider coupling between phytoplankton, nutrients, and zooplankton, which are necessary to capture a full annual cycle. In the context of ecological models, the spring bloom can be described as the period when the ecological system is far from equilibrium (Evans and Parslow 1985). Our analysis is restricted to the period of disequilibrium, when grazing and other pressures cannot compete with the phytoplankton growth.

The following Theory section examines solutions to an idealized phytoplankton model to illustrate when the rate of turbulent mixing becomes an important factor in predicting bloom conditions and to predict the population growth and decay rates in terms of the mixing-layer depth and a turbulent diffusivity. In the Analysis section we then link the turbulent diffusivity to atmospheric forcing in convective conditions and we show how blooms can be triggered by weak forcing. High-resolution numerical simulations are used to show that the critical turbulent diffusivity and the onset of phytoplankton blooms can be linked to the atmospheric forcing. The Discussion presents the implications of our results for the onset of spring blooms in the ocean.

Theory — Turbulent Mixing and the Onset of Spring Blooms

The onset of a bloom triggered by weak atmospheric forcing can be described in terms of the relevant physical and biological timescales. In deep mixed layers, phytoplankton cells will generally multiply faster near the surface where light is abundant, while turbulence counteracts the resulting accumulation of cells by mixing them in the vertical direction. The competition between mixing and local growth can be quantified in terms of two timescales, τ_P and τ_M, associated with phytoplankton growth and turbulent mixing, respectively. When $\tau_M \ll \tau_P$, turbulent mixing acts much faster than net growth and maintains a uniform phytoplankton concentration in the mixing layer, in accordance with Sverdrup's assumption. On the other hand, when $\tau_P \ll \tau_M$ turbulent mixing will not be able to overcome vertical variations in the net growth rate, resulting in a bloom.

The concept of a critical turbulent diffusivity needed to trigger a bloom was first introduced by Huisman et al. (1999) and further developed by Huisman et al. (2002), Ebert et al. (2001), and Ghosal and Mandre (2003). In this section, we extend the earlier work on critical turbulence in three ways. We use a two-layer phytoplankton model to derive an explicit expression for the critical diffusivity in terms of the mixing-layer depth and the phytoplankton growth and loss rates. We then use this result to determine the critical atmospheric forcing needed to trigger a bloom. We also present an analytical solution for the rate of net growth or loss in the phytoplankton population given the depth and intensity of turbulent mixing and biological parameters. This extends the work of Ebert et al. (2001), who primarily focused on steady-state solutions.

We use the following equation to model the early stages of a phytoplankton bloom event:

$$\frac{\partial P(z,t)}{\partial t} = \mu(z,t,P,N)P(z,t) - m(z,t,P,Z)P(z,t) + \frac{\partial}{\partial z}\left(\kappa_T(z,t)\frac{\partial P(z,t)}{\partial z}\right), \quad (2)$$

where P is the phytoplankton concentration, and the local growth rate, μ, loss rate, m, and turbulent diffusivity, κ_T are prescribed functions. Vertical motion of the phytoplankton cells relative to the fluid through sinking and buoyancy or swimming are not explicitly included in Eq. 2, which is a good assumption if the phytoplankton cells are neutrally buoyant and nonmotile, or if the turbulence is strong enough to overcome the relative motion of the cells (Riley 1946; Huisman et al. 2002). If we were interested in the phytoplankton growth over longer (i.e., monthly or seasonal) timescales, Eq. 2 would have to be coupled to additional equations for the nutrients (N), and zooplankton (Z; Evans and Parslow 1985). Instead, we focus on the early stages of the spring bloom when phytoplankton growth is very rapid, before nutrients become depleted and before the zooplankton population has time to respond. We, therefore, assume that μ and m are constant in time over the period of interest (i.e., days to weeks).

In order to simplify the analysis of Eq. 2 we make several additional assumptions, largely following those made by Sverdrup (1953). Specifically, we assume that the growth rate, μ, depends only on the daily-averaged light level at each depth. We are interested in the phytoplankton growth over a short time period; therefore, the daily-averaged light intensity and μ are assumed to be constant in time. By assuming that μ is constant in time, we effectively neglect self-shading effects, which have been included in several previous studies (Huisman et al. 1999; Ebert et al. 2001). Self-shading occurs when the phytoplankton concentration becomes large, and here we focus on the early stages of the bloom when the concentration is still relatively dilute. We further follow Sverdrup (1953) and assume that the loss rate, m, is constant in the mixing layer. This does not allow the loss rate through predation to decrease when the phytoplankton concentration becomes dilute, as predicted by Behrenfeld (2010), or to increase when the phytoplankton become more abundant in the spring, but these effects are likely to occur on longer timescales than those of interest here. Turbulent mixing is represented as a diffusive process using a constant turbulent diffusivity, κ_T, but in the Analysis section, we present results from numerical simulations that do not require this assumption. In the Web Appendix (www.aslo.org/lo/toc/vol_56/issue_6/2293a.pdf), we show how to solve Eq. 2 in a more general framework where μ, m, and κ_T can be arbitrary functions of depth.

Departures from Sverdrup's critical depth theory occur when turbulence is too weak to maintain the concentration of phytoplankton within the mixing layer. In particular, when the phytoplankton growth rate is limited by light exposure, weak turbulence results in higher concentrations of phytoplankton cells near the surface where light is more abundant. By concentrating near the surface, the phytoplankton population preferentially samples a region with abundant light, and the growth rate of the integrated phytoplankton population in the mixing layer is higher than if the cells were evenly exposed to the mean light level. It is, therefore, possible to have a growing nonuniform phytoplankton population in a region that is deeper than the critical depth identified by Sverdrup. In fact, when the turbulent mixing rate is below a critical value, it is even possible to maintain a steady population in an arbitrarily deep mixing layer (Huisman et al. 1999).

a. Simple model—In order to illustrate how nonuniform phytoplankton distributions can lead to larger population growth rates, consider separating the mixing layer into two sublayers about a depth, h. An equivalent two-layer profile of the 'local net growth rate,' $\mu - m$, is illustrated in Fig. 1. The upper layer is meant to represent the euphotic layer where light is abundant, while the lower layer represents the fraction of the mixing layer that receives little light. In the upper layer (layer 1) spanning the region $-h < z < 0$, we assume that local growth dominates over losses at some effective rate μ_{eff} given by appropriate averaging of $\mu - m$. In the lower layer (layer 2) for $-H < z < -h$, we assume that losses dominates local growth with an effective rate m_{eff}. The two layers experience the same mixing set by the

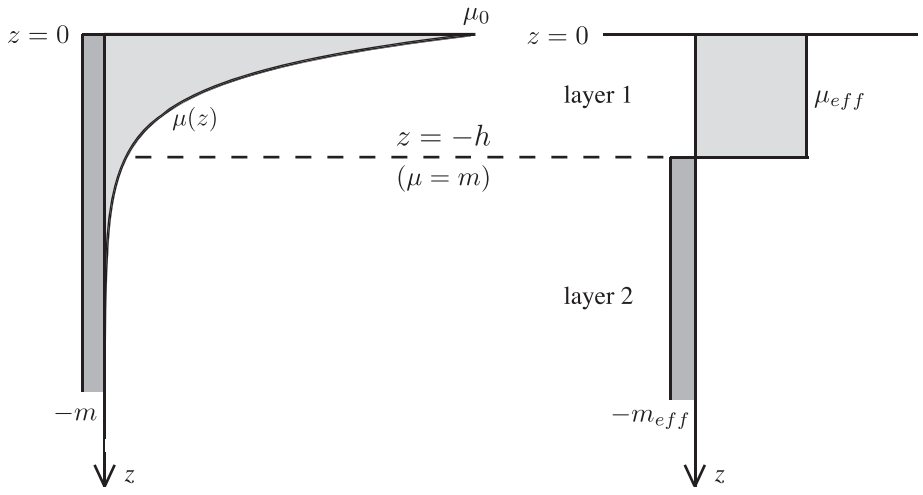

Fig. 1. Schematic showing typical profiles for the local growth rate (μ) and loss rate (m; left), and a simplified system with a piece-wise constant net growth rate used in Eqs. 3–15.

turbulent diffusivity κ_T. Depending on the relative rates of mixing vs. local growth and losses, the phytoplankton concentration in the two layers can be different or equal, and this will translate into two different criteria for the onset of blooms.

The timescales, $\tau_{M,1}$ and $\tau_{M,2}$ associated with turbulent mixing in the upper and lower layers, respectively, can be defined in terms of the layer depth and the turbulent diffusivity, κ_T:

$$\tau_{M,1} \equiv \frac{h^2}{\kappa_T}, \quad \tau_{M,2} \equiv \frac{(H-h)^2}{\kappa_T} \tag{3}$$

while the timescales associated with the effective local growth and loss rates in the two layers are

$$\tau_{P,1} \equiv \frac{1}{\mu_{eff}}, \quad \tau_{P,2} \equiv \frac{1}{m_{eff}}. \tag{4}$$

Critical depth criterion—In the limit of strong turbulence when the mixing timescales are much smaller than the effective growth and loss timescales defined above:

$$\tau_{M,1} \ll \tau_{P,1}, \quad \text{and} \quad \tau_{M,2} \ll \tau_{P,2} \tag{5}$$

and the phytoplankton concentration will be well-mixed in the vertical. Integrating over the two layers and assuming that the vertical phytoplankton flux vanishes at $z = 0$ and the base of the mixing layer, Eq. 2 reduces to

$$\int_{-H}^{0} \frac{\partial P}{\partial t} dz = h\mu_{eff} P - (H-h) m_{eff} P \tag{6}$$

The integrated phytoplankton concentration can grow in time as long as

$$H \le H_C \equiv h\left(\frac{\mu_{eff}}{m_{eff}} + 1\right) \tag{7}$$

(i.e., the mixing-layer depth must be shallower than a critical depth H_C, consistent with Sverdrup's theory).

Critical turbulence criterion—The weak turbulence limit first becomes relevant in late winter or early spring when the mixing-layer depth is typically much deeper than the layer with positive net growth: $H \gg h$. In this case, inspection of Eq. 3 reveals that the mixing time is much longer in the lower layer than the upper layer. Therefore, for moderate turbulence levels, turbulence may be sufficient to fully mix the upper layer, but not the lower layer, i.e.,

$$\frac{h^2}{\kappa_T} \ll \frac{1}{\mu_{eff}}, \quad \text{and} \quad \frac{(h-H)^2}{\kappa_T} \sim \frac{1}{m_{eff}}. \tag{8}$$

In this limit there is a critical turbulence level, κ_C, below which growth in the phytoplankton population can occur regardless of the mixing-layer depth. This critical level is found by looking for steady-state solutions of Eq. 2. Based on Eq. 8, turbulent mixing still dominates in the upper layer, so the phytoplankton concentration will remain uniform near the surface. However, we can no longer assume that the phytoplankton are uniform in the lower layer. There, the effective loss rate is balanced by a downward flux of cells driven by

$$\kappa_T \frac{\partial^2 P_2}{\partial z^2} - m_{eff} P_2 = 0. \tag{9}$$

The solution to Eq. 9 is

$$P_2(z) = Ce^z \sqrt{m_{eff}/\kappa_T} \tag{10}$$

where C is an arbitrary constant. The solution in the upper layer is uniform and must match P_2 at the interface at $z = -h$; hence,

$$P_1 = Ce^{-h} \sqrt{m_{eff}/\kappa_T}. \tag{11}$$

At the critical turbulence threshold, the net phytoplankton growth in the upper layer is balanced by the downward flux of cells into the lower layer by turbulent mixing. An

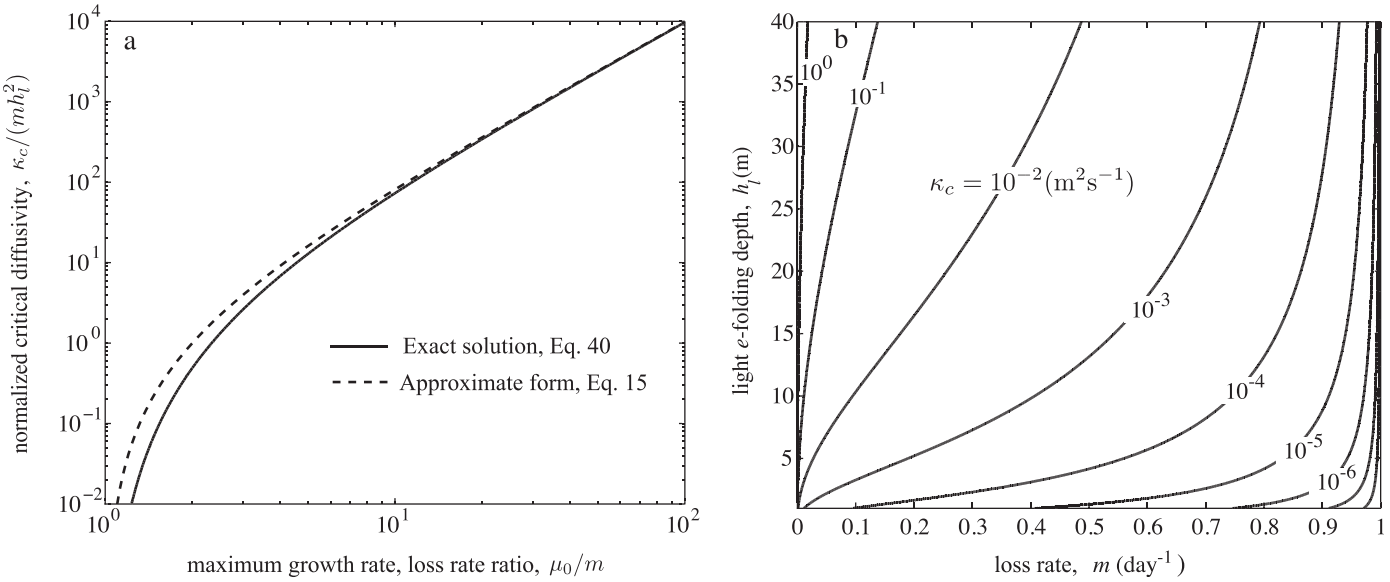

Fig. 2. (a) Comparison of the normalized critical diffusivity, as a function of local growth and loss rate ratio, $\mu^* = \mu_0 / m$ for the exact solution given in Eq. 40 and the approximate form in Eq. 15. (b) Critical diffusivity as a function of the loss rate (m), and the e-folding depth associated with the local growth rate (h_l) for a fixed maximum local growth rate, $\mu_0 = 1$ d^{-1} from Eq. 15.

expression for the critical turbulence level can be obtained by matching the integrated growth rate in the upper layer with the flux into the lower layer,

$$\int_{-h}^{0} \mu_{eff} P_1 dz = \kappa_T \frac{\partial P_2}{\partial z}\bigg|_{-h}. \tag{12}$$

Substituting the steady-state solutions for P_1 and P_2 into Eq. 12 provides an expression for the critical turbulent diffusivity in terms of the other parameters,

$$\kappa_T = \kappa_C \equiv \frac{h^2}{m_{eff}} \mu_{eff}^2. \tag{13}$$

The critical turbulence level, κ_C is the minimum turbulent diffusivity required to flux phytoplankton out of the euphotic layer fast enough to keep up with local growth. When $\kappa_T < \kappa_C$, phytoplankton cells accumulate near the surface where μ is large, and when $\kappa_T > \kappa_C$ the flux of phytoplankton cells into the lower layer is larger than the effective growth rate in the upper layer and the number of living cells decays.

Thus far, we have assumed that local phytoplankton growth can be represented by a constant effective net growth rate, μ_{eff}, acting over a layer of thickness h. In general, the growth rate, μ, will vary continuously throughout the water column. Among other factors, μ will depend on the average light made available to each cell, which, in turn, depends on depth. For example, a model growth-rate profile can be set by assuming that the growth rate increases linearly with the light intensity, and that the light decays exponentially with depth following Lambert–Beer's law. If we also assume that the loss rate is constant, following Sverdrup (1953), then

$$\mu(z) = \mu_0 e^{-z/h_l}, \quad m = \text{constant} \tag{14}$$

where μ_0 is the maximum local growth rate at $z = 0$, and h_l sets the depth of light penetration. Details of the full solution to Eq. 2 with this form for μ and m will be given in the next section, but it is useful to have a simple, explicit expression for κ_C. One approximation to the critical diffusivity in this case can be obtained by using $h = h_l$ as the characteristic depth, the surface growth rate for the upper layer growth rate, $\mu_{eff} = \mu_0 - m$, and the constant loss rate, $m_{eff} = m$, in Eq. 13:

$$\kappa_C \simeq \frac{h_l^2}{m}(\mu_0 - m)^2. \tag{15}$$

The critical turbulence level is proportional to the square of the light penetration depth, h_l, as suggested by Huisman et al. (1999). Figure 2a shows a comparison of the approximate critical turbulence level using Eq. 15 to the exact solution first derived by Ebert et al. (2001) and described in the next section and in the Web Appendix. Eq. 15 provides an excellent approximation to the exact solution. Figure 2b shows contours of κ_C from Eq. 15 for $\mu_0 = 1$ d^{-1} as a function of m and h_l.

b. General solution—In the previous section, we considered steady-state solutions for a piece-wise constant net growth rate. It is possible to obtain solutions under more realistic conditions. In the limit of strong mixing considered by Sverdrup (1953), the achieved growth rate is equal to the vertical average of the local net growth rate over the mixing layer, $\sigma = (1/H)\int_{-H}^{0}(\mu - m)dz$. For finite turbulence levels, this is no longer true because the vertical distribution of phytoplankton cells becomes important, and σ will depend on the depth and *intensity* of mixing.

A method for finding the achieved growth rate for a given set of biological and physical parameters is outlined in the Web Appendix. Given an initial phytoplankton

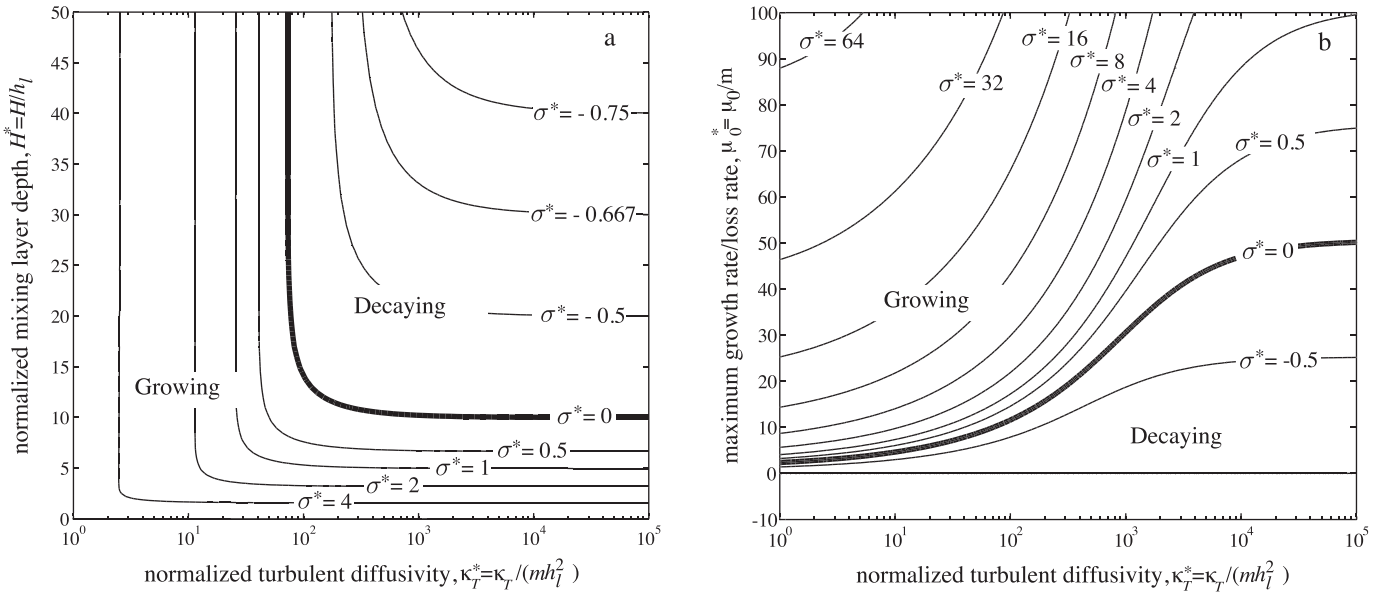

Fig. 3. Normalized maximum achieved growth rate, $\sigma^* = \sigma / m$, as a function of (a) the turbulent diffusivity, $\kappa_T^* = \kappa_T / m h_1^2$, and mixing-layer depth, $H^* = H / h_1$ for $\mu_0^* = \mu_0 / m = 10$, and (b) as a function of κ_T^* and μ_0^* for $H^* = 50$. The achieved growth rate has been found by solving Eq. 2 with no flux boundary conditions at the surface ($z = 0$) and base of the mixing layer ($z = -H$).

concentration, and an appropriate set of boundary conditions, $P(z, t)$ can be written as the sum of a series of modes, each with a particular depth dependence and an associated achieved growth rate, σ_n. The instantaneous achieved growth rate, σ, can be then calculated by combining the solutions for each mode. However, under bloom conditions, when the phytoplankton population is growing exponentially, we expect P to eventually become dominated by the most rapidly growing mode so that the achieved growth rate asymptotes $\sigma \rightarrow \max(\sigma_n)$. An important feature of the solution for the maximum achieved growth rate, σ, is that it is independent of the initial conditions. This means that the conditions for bloom development depend exclusively on measurable physical and biological parameters.

Figure 3a shows the maximum achieved growth rate normalized by the constant loss rate, $\sigma^* = \sigma / m$, as a function of the nondimensional turbulent diffusivity and mixing-layer depth, $\kappa_T^* = \kappa_T / (m h_l^2)$ and $H^* = H / h_l$. Here, the growth and loss rates follow the form in Eq. 14. The vertical phytoplankton flux is assumed to be zero at the ocean surface ($z = 0$) and at the base of the mixing layer ($z = -H$). Normalizing by m and h_l, we have reduced the number of free parameters in the problem from five to three, allowing a wider range of parameters to be shown in each figure. The thick black lines in Fig. 3 separate growing and decaying solutions. For large κ_T^*, the critical condition with $\sigma^* = 0$ is only a function of H^* as surmised by Sverdrup. But for large H^*, the critical condition is only a function of κ_T^*, consistent with Huisman's critical turbulence argument. The maximum achieved growth rate also depends on the biological response through $\mu_0^* = \mu_0 / m$, as illustrated in Fig. 3b for a relatively deep mixing layer with $H^* = 50$. Again, the thick black line shows the neutral solution with $\sigma^* = 0$. In the limit of $\kappa_T^* \rightarrow \infty$, the steady solution with $\sigma^* = 0$ becomes identical to Sverdrup's critical depth with $\mu_0 / m = H_C / h_l = 50$.

A distinguishing feature of the blooms predicted in the critical turbulence limit is that the phytoplankton growth is higher near the surface, where the net growth rate is maximum. The vertical structure of the steady-state phytoplankton concentration is shown in Fig. 4a for $\sigma^* = 0$ and $\mu_0^* = 10$ for various values of κ_T^*. The vertical turbulent phytoplankton flux is also shown in Fig. 4b, normalized by the integrated growth rate. The shaded region indicates where $\mu(z) > m$, above the compensation depth. For large values of κ_T^*, the phytoplankton profiles are nearly uniform in the vertical, consistent with the assumption made by Sverdrup. As κ_T^* approaches the critical turbulence level, the phytoplankton concentration approaches zero at depth and the profile becomes more surface-intensified. In this case, the added net loss at deep levels is compensated for by extra net growth near the surface.

The solution given in Eq. 37 of the Web Appendix can be modified to allow for a flux of phytoplankton at the base of the mixing layer, and this can be seen graphically using Fig. 4. A flux of phytoplankton cells out of the mixing layer will require a shallower mixing-layer depth in order to maintain a steady state. For example, consider the steady-state solutions shown in Fig. 4 for the case when $\kappa_T^* = 1000$, indicated by long dashed lines. If we prescribe a no flux boundary condition at the base of the mixing layer, $z = -H$, then based on Fig. 4b, the critical depth is $H_C^* \simeq 10$ or $H_C / h_l \simeq \mu_0 / m$ in agreement with Sverdrup's theory. On the other hand, if there is a downward flux of phytoplankton at the base of the mixing layer at a rate of, say 20% of the integrated growth, then the steady-state mixing-layer

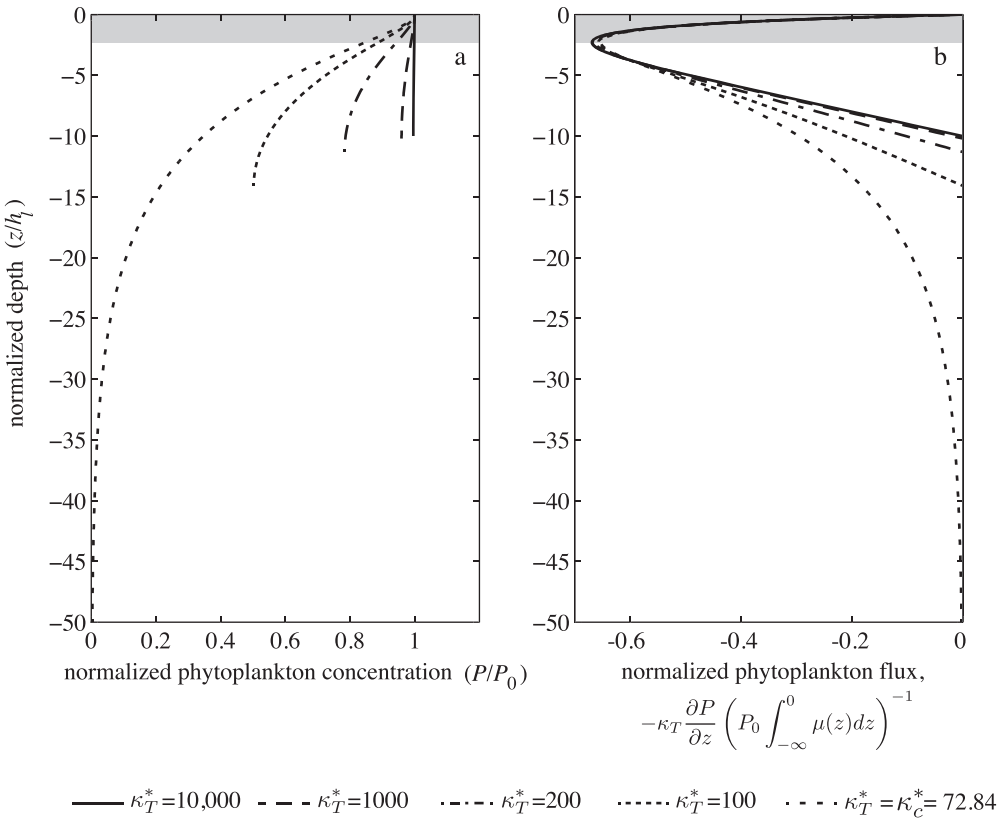

Fig. 4. (a) Vertical profiles of the nondimensional phytoplankton concentration from the analytical solution Eq. 37 with $\mu_0 = 1\ \mathrm{d}^{-1}$, $m = 0.1\ \mathrm{d}^{-1}$, and $\partial P / \partial z(z = 0) = 0$. (b) Profiles of the nondimensional turbulent phytoplankton flux.

depth becomes $H_c^* \simeq 8$. The steady-state mixing-layer depth is even more sensitive to the phytoplankton flux for smaller values of κ_T^*.

Analysis — Critical Turbulence and Critical Forcing Levels

The turbulent diffusivity introduced in Eq. 2 will depend on both the depth and intensity of the turbulent mixing. In this section, we use the following framework to relate the turbulent diffusivity to the atmospheric forcing. First, based on mixing length theory, the turbulent diffusivity can be expressed in terms of a turbulent velocity scale (w^*) and a length-scale (l): $\kappa_T \sim w^* l$. In the turbulent boundary layer, w^* can be related to the atmospheric forcing, while l characterizes the length-scale of the most energetic turbulent motions. Scaling laws for w^* and l ultimately lead to an expression for the critical atmospheric forcing and the prediction that the onset of the spring bloom will occur when the forcing becomes weaker than the critical level.

A wide variety of physical mechanisms generate turbulence in the ocean including wind, breaking surface and internal waves, Langmuir circulation, surface heat and salt fluxes, etc. (e.g., Thorpe 2005). Here, we do not attempt to address the contributions from all of these processes on phytoplankton growth. Instead, we focus on turbulence generated by thermal convection when the surface of the ocean is cooled. This is motivated by our desire to consider the conditions leading to the onset of the spring bloom after deep winter mixed layers are generated by intense surface cooling.

For turbulence forced by thermal convection in a nonrotating environment, the following scaling has been verified by numerous laboratory experiments (Deardorff and Willis 1985; Fernando et al. 1991), and numerical simulations (Deardorff 1972; Molemaker and Dijkstra 1997)

$$l \sim H, \quad w_* \sim |HB_0|^{1/3}, \tag{16}$$

where $B_0 = \kappa \partial b / \partial z|_{z=0}$ is the surface buoyancy flux. The buoyancy, b, is related to the fluid density, ρ, according to $b = -g\rho / \rho_0$, where ρ_0 is a reference density and g is the gravitational acceleration. Using the length and velocity scale in Eq. 16, the turbulent diffusivity due to convective motions is expected to scale as

$$\kappa_T \sim l w_* = C H^{4/3} |B_0|^{1/3}, \tag{17}$$

where C is an empirical scaling constant (Send and Marshall 1995; Klinger et al. 1996). When the surface density is only affected by temperature changes, the surface buoyancy flux, B_0 can be related to the surface heat flux

$$Q_0 = c_P \rho_0 B_0 / (\alpha g), \tag{18}$$

where c_P is the heat capacity, α is the thermal expansion

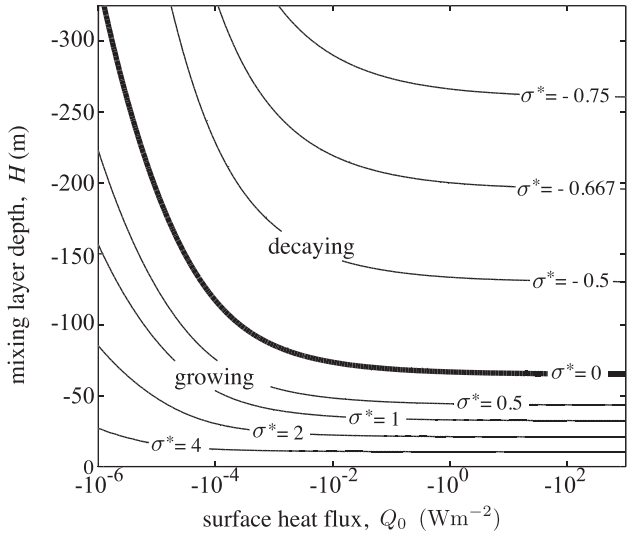

Fig. 5. Predicted maximum achieved growth rate, $\sigma^* = \sigma / m$ as a function of the surface heat flux (Q_0) and the mixing depth (H). Predictions are based on Eq. 19 with the following parameter values: $\mu_0 = 1\ \mathrm{d}^{-1}$, $m = 0.1\ \mathrm{d}^{-1}$, $h_1 = 6.5$ m, $c_P = 4 \times 10^3$ J / (kg °C), $\alpha = 1.65 \times 10^{-4}\mathrm{°C}^{-1}$, $g = 9.81\ \mathrm{m^2\ s^{-1}}$, $\rho_0 = 1000\ \mathrm{kg\ m^{-3}}$, and $C = 1 / 5$.

coefficient, ρ is the water density, and g is the gravitational acceleration. The turbulent diffusivity can then be written directly in terms of the surface heat flux:

$$\kappa_T = CH^{4/3}\left|\frac{\alpha g}{\rho_0 c_P} Q_0\right|^{1/3}. \tag{19}$$

Equation 19 only applies under convective conditions when $Q_0 < 0$, indicating net cooling of the ocean surface.

Based on the scaling above, we can reformulate the critical turbulent diffusivity in Eq. 15 to obtain an expression for the 'critical heat flux':

$$Q_C \simeq -\frac{1}{C^3}\frac{c_P\rho_0}{\alpha g}\frac{h_1^6(\mu_0 - m)^6}{m^3 H^4}. \tag{20}$$

When $|Q_0| > |Q_C|$, convectively driven turbulence will be sufficient to keep the phytoplankton concentration uniformly distributed, and Sverdrup's critical depth hypothesis is valid, whereas when $|Q_0| < |Q_C|$, convectively driven turbulence is insufficient to redistribute the phytoplankton across the mixing layer, and we expect to see the phytoplankton population grow near the surface. Unlike the critical diffusivity, the critical heat flux depends on the depth of the convective mixing layer, H. The achieved growth rate, σ, is plotted as a function of the surface heat flux and the mixed-layer depth in Fig. 5 for $\mu_0 = 1\ \mathrm{d}^{-1}$ and $m = 0.1\ \mathrm{d}^{-1}$. Significant departures from Sverdrup's theory are only felt for very small values of the surface heat flux, in this case for $|Q_0| < O(1\ \mathrm{W\ m^{-2}})$. For all practical purposes, this threshold is indistinguishable from $|Q_C| = 0$.

The above analysis assumes that thermal convection driven by cooling of the ocean surface is the dominant source of turbulence. Using Eq. 18, the critical heat flux in Eq. 20 can be rewritten as a critical buoyancy flux, and this should be used instead when evaporation, precipitation, river runoff, or ice-melt lead to a significant freshwater flux. During winter, we expect convection to dominate over wind-driven turbulence in deep mixing layers. Specifically, convection is expected to dominate wind forcing below the Obukhov length, $z < -L_{Ob}$, where

$$L_{Ob} = \frac{-u_*^3}{\kappa B_0}, \tag{21}$$

where $u_* = (\tau_w / \rho_0)^{1/2}$ is the friction velocity, τ_w is the wind stress, and $\kappa = 0.41$ is the von Karman constant. For typical values in the subpolar gyre of the North Atlantic in winter, say $u_* = 0.015\ \mathrm{m\ s^{-1}}$, $B_0 = 1 \times 10^{-7}\ \mathrm{m^2\ s^{-3}}$, the Obukhov length is $L_{Ob} \simeq 82$ m. This is generally shallower than the mixed-layer depth at high latitudes; therefore, we expect convection to dominate the deep mixing of phytoplankton under these conditions.

The scaling used in Eqs. 16–19 does not account for the influence of the Earth's rotation. Rotation strongly affects convection when the convective Rossby number is small,

$$Ro_* = \left(\frac{B_0}{f^3 H^2}\right)^{1/2} \ll 1, \tag{22}$$

where f is the Coriolis parameter (Klinger et al. 1996; Levy and Fernando 2002). For the cases that we consider here in our simulations, the effect of rotation is indeed small. For example, when $Q_0 \simeq -100\ \mathrm{W\ m^{-2}}$, $H \simeq 100$ m, $f \simeq 1 \times 10^{-4}\ \mathrm{s^{-1}}$, the convective Rossby number is $Ro_* \simeq 2$. Rotational effects can becomes important for very deep convective layers (Klinger et al. 1996), but because the surface heat flux is strong during deep convection events, it seems unlikely that the critical turbulence criteria would be met in this limit.

c. Numerical simulations—In order to test the predictions from the theory outlined in the previous sections and to examine how a diffusive parameterization of turbulent mixing relates to realistic forcing conditions, we have conducted a series of high-resolution three-dimensional numerical simulations of turbulence in the upper ocean. In the previous section, we considered a one-dimensional phytoplankton model where turbulent mixing was represented by a constant turbulent diffusivity. More generally, the concentration of phytoplankton cells and the turbulent diffusivity can vary in all three spatial dimensions and time. If we make the same assumptions as before regarding the biological response, then the phytoplankton concentration will satisfy the following equation:

$$\frac{\partial P}{\partial t} + \mathbf{u}\cdot\nabla P = (\mu(z) - m)P + \kappa\nabla^2 P, \tag{23}$$

where the second term on the left-hand side represents advection by the three-dimensional velocity field and κ is the diffusivity due to random motions of the phytoplankton cells. This latter term will almost always be small compared to advection by turbulence, so we will neglect it here. Averaging Eq. 23 over horizontal planes and assuming periodic lateral boundary conditions (consistent

Table 1. Parameters for large-eddy simulations of steady convection. The simulations resolve the domain size of Lx, Ly, Lz, using Nx, Ny, Nz computational grid-points. Other parameters are described in the text.

H (m)	N_∞ (s^{-1})	Q_0 (W m^{-2})	μ_0 (d^{-1})	m (d^{-1})	h_l (m)	Lx, Ly, Lz (m)	Nx, Ny, Nz
50	9.5×10^{-3}	$-1, -10, -100, -1000$	1	0.1	5	200, 200, 100	192, 192, 100

with our numerical simulations) gives the following equation for the mean phytoplankton concentration:

$$\frac{\partial \langle P \rangle}{\partial t} + \frac{\partial}{\partial z}\langle w'P' \rangle = (\mu(z) - m)\langle P \rangle, \tag{24}$$

where $\langle \cdot \rangle$ denotes a horizontal average and primes denote departures from this average. In order to solve Eq. 24, for the mean phytoplankton concentration profile, we need some knowledge of the vertical turbulent flux, $\langle w'P' \rangle$. One common approach is to assume that the flux is always directed down the mean gradient. In this case, we can define a positive turbulent diffusivity, κ_T, where

$$\kappa_T \equiv \frac{-\langle w'P' \rangle}{\partial \langle P \rangle / \partial z}. \tag{25}$$

Substituting Eq. 25 into Eq. 23, one recovers the phytoplankton model we considered in the Theory section, except for the fact that κ_T is not necessarily constant in depth and time. In this section, we use three-dimensional numerical simulations to calculate the advective flux and diagnose the turbulent diffusivity from Eq. 25.

The computational method that we have used is known as large-eddy simulation (LES). The distinguishing feature of LES is that the largest, most energetic turbulent eddies are explicitly resolved. We are interested in quantifying turbulent mixing and its effect on phytoplankton growth; therefore, this problem is well-suited for LES instead of other methods that fully parameterize the turbulent mixing. The LES model is used to solve both the equations for the three-dimensional velocity field **u** and for the phytoplankton concentration P. Details of the numerical method are given in Taylor and Ferrari (2010) and Taylor (2008).

In each simulation, turbulence is generated by imposing a constant, negative surface heat flux. To simulate a wide range of conditions seen in the ocean, we ran simulations with the surface heat flux varying from -1 to -1000 W m^{-2}. The density field was initialized with a mixed layer equal to Sverdrup's critical depth, $H(t = 0) = H_C = 50$ m. Below the mixed layer, the density field was linearly stratified with a buoyancy frequency, N_∞, where $N_\infty^2 \equiv (-g/\rho_0)\partial\rho/\partial z$, and ρ_0 is the background density used in the Boussinesq approximation. The phytoplankton concentration is initially uniform over the computational domain, $P = P_0$. The surface heat flux is imposed as a boundary condition on the temperature equation at $z = 0$, and the value of the surface heat flux is linearly increased from zero to the maximum value over the period of a day, after which it is held constant. The parameters for this set of simulations are given in Table 1.

Convective cells develop in the mixed layers in all simulations, even when $Q_0 = -1$ W m^{-2}. Figure 6 shows the normalized phytoplankton concentration for this case. Green indicates concentrations larger than the initial value, and blue indicates weaker concentrations. Convective cells are visualized using white streamlines. The spatial distribution of phytoplankton is clearly correlated with the convective structures. High phytoplankton concentrations are seen in the downwelling regions and low concentrations in the upwelling regions. This is the opposite of what might be expected under nutrient-limited conditions, but a downward net flux of phytoplankton is consistent with turbulence mixing a surface-intensified mean phytoplankton profile as seen in this case under light-limited conditions (Fig. 7).

We can now calculate the turbulent diffusivity as defined in Eq. 25, using the three-dimensional velocity field and the phytoplankton concentration from the numerical simulations to estimate the turbulent phytoplankton flux, $\langle w'P' \rangle$, and mean phytoplankton concentration, $\langle P \rangle$. Profiles of the turbulent diffusivity are shown in Fig. 8 for each simulation. As the magnitude of the surface heat flux is increased, the turbulence becomes more energetic and κ_T increases. The scaling of κ_T with the surface heat flux is well-captured by the scaling theory. The dotted lines in Fig. 8 show Eq. 19 with an empirical scaling constant of $C = 1/5$.

In the Theory section, we saw that the phytoplankton concentration can become surface-intensified when turbulent mixing is weak. The degree of depth-dependence of the phytoplankton concentration depends on the level of mixing, with more surface intensification when κ_T is near

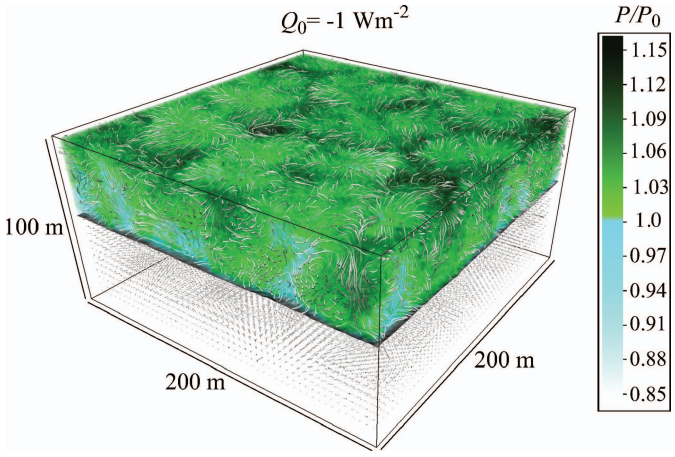

Fig. 6. Visualization of the phytoplankton concentration from the large-eddy simulation with a surface heat flux of $Q_0 = -1$ W m^{-2}. The density surface bounding the base of the mixed layer is shown in gray and instantaneous streamlines are shown in white.

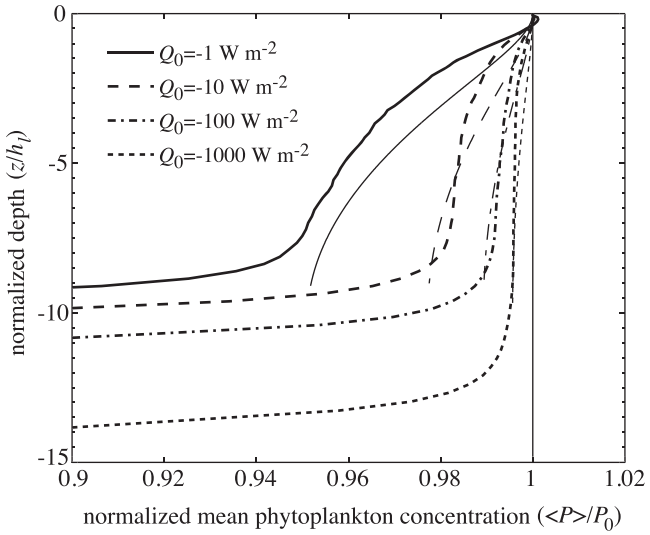

Fig. 7. Profiles of the plane-averaged phytoplankton concentration from the large-eddy simulations at $t = 1.5$ d. The prediction from the analytical solution using the prescribed heat flux and the mixed-layer depth from the simulation are shown using thin lines for comparison. The mixed-layer depth is defined as the location where $\langle N^2 \rangle = 0.01 N_\infty^2$.

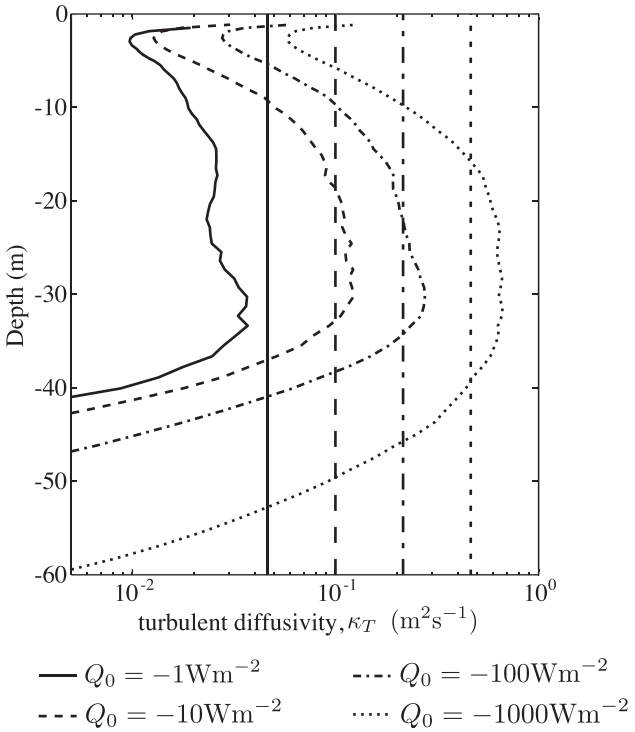

Fig. 8. Turbulent diffusivity, κ_T, for phytoplankton, inferred from large-eddy simulations forced with a constant surface heat flux (Q_0). Equation 25 is used to calculate profiles of κ_T where the averaging operator denoted by angle brackets in Eq. 25 is defined as an average over horizontal planes and in time from $1 \leq t \leq 1.5$ d. Vertical lines show the κ_T predicted from Eq. 19. Only the resolved scale motions contribute significantly to the advective flux in κ_T. The sub–grid-scale and molecular diffusivities are much smaller than κ_T in all cases.

the critical turbulence level (*see* Fig. 4). We can test the predicted analytical solutions by comparing with the simulations of phytoplankton in turbulent convection. Figure 7 shows the phytoplankton concentration from the LES averaged over horizontal planes at $t = 1.5$ d. The analytical solutions from Eq. 37 are shown in dashed lines for comparison. To plot the analytical solution, the turbulent diffusivity was estimated from the surface heat flux using Eq. 19. Because turbulence extends to the base of the mixed layer in these simulations of active convection, the mixed-layer depth is a good proxy for the mixing depth, and H is defined as the location where $\langle N^2 \rangle = 0.01 N_\infty^2$. It is worth noting that the theoretical prediction uses only commonly measured quantities: the surface heat flux, Q_0 and the density profile, $\rho(z)$. In general, the analytical solutions capture the depth-dependence seen in the LES very well. The profiles of the phytoplankton concentration from the LES tend to have steeper gradients than the analytical solution in the upper portion of the convective layer. This is probably due to the fact that the analytical solutions use a constant turbulent diffusivity, while κ_T was weaker near the surface in the LES (*see* Fig. 8).

We have seen that when the atmospheric forcing is very weak, phytoplankton blooms can form in deep mixed layers. But how quickly can phytoplankton respond to changes in the forcing conditions? To address this question, we ran a simulation of turbulent convection and gradually increased the surface heat flux (so that Q_0 went from large and negative up to zero). The goal of this simulation was to examine how phytoplankton respond to changes in the forcing conditions. In nature, these changes occur on both synoptic and seasonal timescales, but it is not computationally feasible to simulate changes in the atmospheric forcing over very long timescales using LES. Instead, we spin-down the surface heat flux over a period of 2 d. Although this is only marginally slower than the maximum local growth rate of 1 d^{-1}, as we will see, the phytoplankton respond quickly to changes in the atmospheric forcing and the results are not compromised by the short duration of the spin-down.

The surface heat flux and the response of the phytoplankton concentration are shown in Fig. 9. The bottom panel shows the integrated phytoplankton concentration above the compensation depth. Because the surface heat flux never becomes positive ($Q_0 \leq 0$), the mixed layer does not restratify in this simulation. Despite the fact that the mixed layer remains deeper than the critical depth (indicated with a dashed line in the middle panel), exponential growth in the phytoplankton population coincides very closely with the time when the net heat flux reaches zero. The concentration of phytoplankton at $z = 0$ actually begins to grow slightly before the net heat flux reaches zero.

The numerical simulations are consistent with the prediction based on the critical turbulence hypothesis that weak atmospheric forcing can trigger phytoplankton blooms. In situations where weak forcing precedes restratification of the mixed layer, the onset of blooms can occur before the mixed layer becomes shallower than the critical

depth, either by a reduction in the depth of the mixing layer or in the intensity of mixing. This implies that the surface heat flux might be a better bulk indicator of the phytoplankton response than the mixed-layer depth. Observational support for this argument is given in the Discussion section.

Notice that when the surface cooling subsides, the turbulence vanishes and, hence, both the critical turbulence and the critical depth criteria are satisfied. However, the mixing layer is slaved to the surface heat flux and not vice-versa. Hence, the surface heat flux is the external controlling process and not a change in the water column. The depth of the mixed layer itself (i.e., the region with weak stratification), hardly changes throughout the simulation because restratification is a slow process. We conclude that the criterion for the onset of a bloom is indeed best expressed in terms of the surface heat flux, as in the critical turbulence argument, and not in terms of a mixing-layer depth, as in Sverdrup's argument.

Discussion

Previous studies have shown that phytoplankton blooms can be triggered by weak forcing, irrespective of the mixed-layer depth (Huisman et al. 1999; Ebert et al. 2001; Ghosal and Mandre 2003). This implies that at least two parameters, the intensity and depth of mixing, are necessary to describe the effect of turbulent mixing on the onset of a phytoplankton bloom. Here, we have extended previous work by deriving an expression for the critical turbulent diffusivity and relating it to a critical surface heat flux under convective conditions. Based on this analysis, we predict that the onset of the spring phytoplankton bloom should closely correspond with the end of convective conditions. We then conducted three-dimensional numerical simulations to test this hypothesis and verified that weak convective forcing can trigger a bloom.

The critical surface heat flux derived in the Analysis section depends on the same set of physical and biological parameters as the critical depth and critical turbulence criteria. Some of these parameters, such as the phytoplankton growth and loss rates, are very difficult to measure in the field. However, as shown in Fig. 5, for most practical situations the critical surface heat flux is not significantly different from zero. This was verified in the simulation shown in Fig. 9 where phytoplankton growth began very close to the time when the surface heat flux was turned off. Based on these results, we predict that the onset of the spring phytoplankton bloom should closely coincide with the time when the seasonal thermal forcing switches from net cooling to net warming of the ocean. The surface heat flux is readily available in global databases; therefore, this prediction should be easily testable using satellite observations or in situ measurements.

Our findings based on the role of the surface heat flux have important practical implications for predicting the onset of a bloom. Measuring the intensity of turbulence requires specialized instrumentation (Gregg 1991). Estimating the turbulent diffusivity is further complicated by the fact that temperature and density gradients are weak in the mixed layer. As a result, the mixed layer is often used as a proxy for where turbulence is strong. During periods of strong forcing, the mixed-layer depth is, indeed, likely to be a good proxy for the mixing depth. However, as we have shown, when the atmospheric forcing becomes weak, turbulence subsides rapidly while the mixed-layer depth does not change much. Shoaling of deep mixed layers is the result of restratification, which occurs on timescales of weeks to months. Therefore, the onset of the bloom can occur significantly prior to the time when the mixed layer restratifies beyond the critical depth. Townsend et al. (1992) and Dale and Heimdal (1999) do indeed report blooms weeks before shoaling of the mixed layer. We are led to conclude that the sign of the net surface heat flux should provide a better indicator for the onset of the spring bloom than the mixed-layer depth alone.

Our hypothesis that the spring bloom should coincide with the end of convective forcing can be tested using readily available data sets. For example, Fig. 10 shows a time-series of chlorophyll concentration obtained from the SeaWiFS satellite, along with the monthly mean net surface heat flux obtained from a National Centers for Environmental Prediction/National Center for Atmospheric Research reanalysis. Shaded regions indicate periods when the surface heat flux is negative. The chlorophyll concentration and heat flux have been averaged over two regions, characterizing the northern (Fig. 10a) and southern (Fig. 10b) limits of the subpolar North Atlantic. Strong bloom events generally closely coincide with the end of net surface cooling, indicating that the sign of the surface heat flux may indeed provide a good indication for the onset of the spring bloom. As shown in Henson et al. (2006, 2009), the spring bloom occurs later at high latitudes, and this delay appears to match the delay in the change in sign of the surface heat flux.

Although the strongest growth events coincide closely with the end of convective forcing, the chlorophyll concentration begins to increase several months earlier, in midwinter. This is consistent with the recent studies by Behrenfeld (2010) and Boss and Behrenfeld (2010), who found that the near-surface chlorophyll concentration starts to increase in midwinter when the mixed-layer depth is at maximum. Using satellite observations and a mixed-layer depth climatology, Behrenfeld (2010) found that the vertically integrated phytoplankton population begins to increase in the late autumn when the mixed layer is still deepening. The exponential growth rate is proportional to the slope of the chlorophyll curves plotted on a logarithmic axis in Fig. 10, and the growth rate associated with the spring bloom is much higher than the earlier growth phase in winter. Because this early growth phase occurs when the surface heat flux is large and negative, it is unlikely to be described by the critical heat flux mechanism described here. Behrenfeld (2010) described this early growth phase using a 'dilution-recoupling' hypothesis, whereby the deepening of the mixed layer reduces the grazing pressure, and the phytoplankton population increases in response. As long as the assumptions described in the Theory section are still valid (e.g., nutrient limitation and self-shading can be neglected), our theory can be applied regardless of

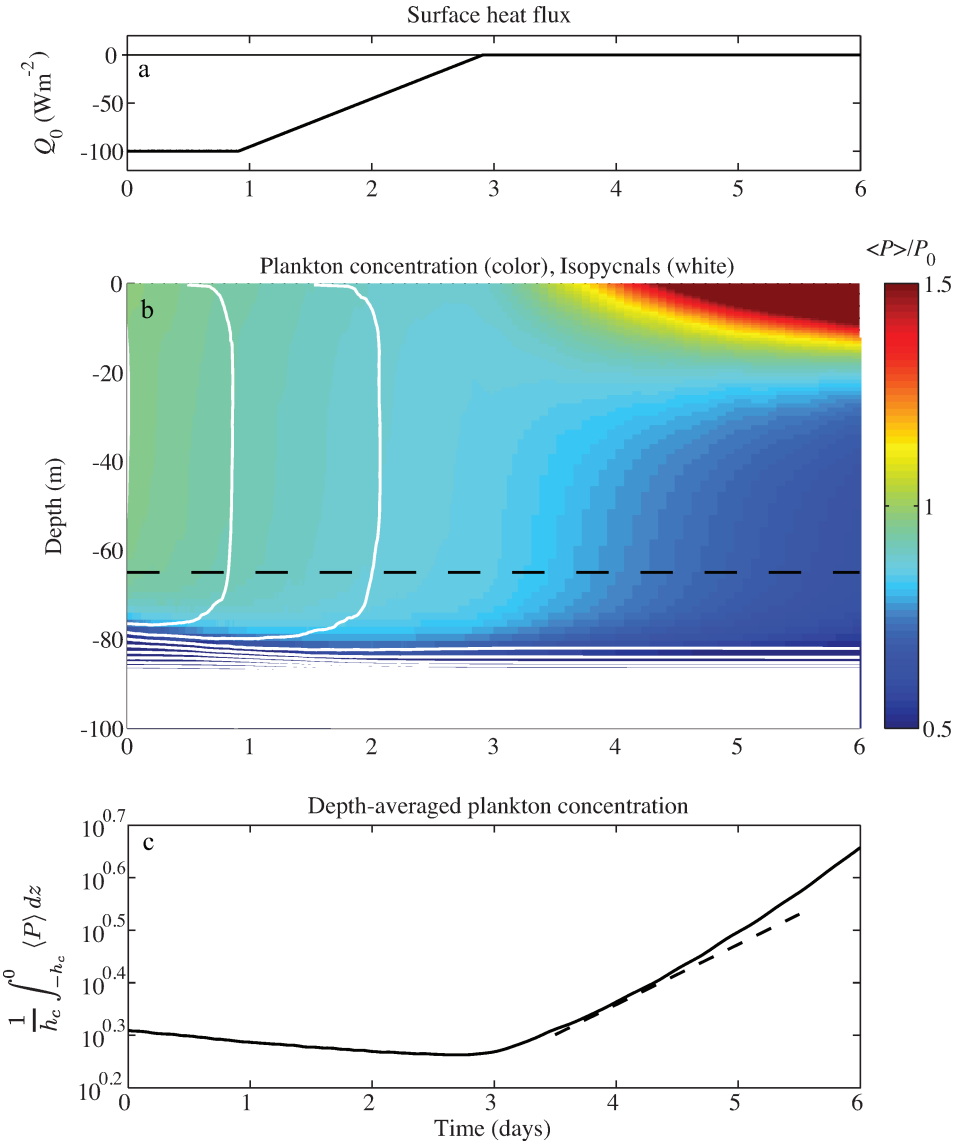

Fig. 9. Phytoplankton response to a reduction in forcing strength, shown in (a), from large-eddy simulations. The parameter values are the same as in Fig. 5. (a) Time evolution of the surface heat flux. (b) The phytoplankton concentration averaged over the horizontal computational domain (color) and constant density contours (white). The critical depth is indicated by the black dashed line. (c) The evolution of the mean phytoplankton concentration above the compensation depth, i.e., the level z such that $\mu(z) = m$. The slope of the black dashed line shows the net growth rate, $\mu - m$, averaged over the same region.

whether the phytoplankton concentration was increasing or decreasing prior to the change in forcing conditions. Based on Fig. 3, a reduction in the turbulent diffusivity will lead to an increase in the achieved growth rate, σ^*, regardless of whether the phytoplankton population was growing or decaying prior to the change in forcing.

Figure 10 shows suggestive new evidence that the timing of the spring bloom is related to the end of wintertime convection, but several factors need to be considered before the theory can be fully evaluated. For example, a surface freshwater flux due to precipitation, river runoff, or ice melt can also contribute to the surface buoyancy flux and may be able to stabilize convection. Turbulence generated by wind and waves can also affect the mixing-layer depth, particularly when the mixed layer is relatively shallow. If the wind-driven turbulence is sufficient to keep the phytoplankton well-mixed below the critical depth, then blooms will be suppressed. Finally, lateral advection can restratify the upper water column and may suppress turbulent mixing, particularly near fronts and eddies with large horizontal density contrasts.

Our results have possible important implications for the overall ocean productivity. When a bloom occurs during a period of weak atmospheric forcing, population growth can be achieved in deep mixed layers. This is in contrast to blooms that occur after the upper ocean restratifies, when

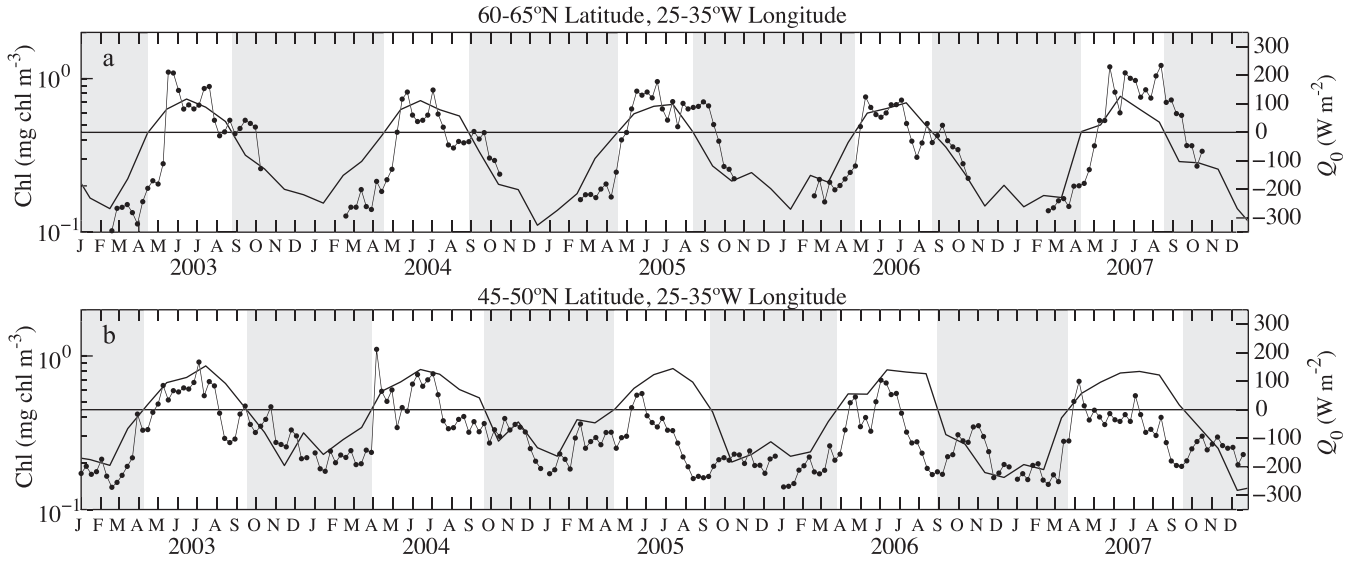

Fig. 10. Chlorophyll concentration estimated from the SeaWiFS satellite (dots) in two regions of the North Atlantic compared with the surface heat flux (thin line). Regions with negative surface heat flux are shaded. Chlorophyll data were provided by S. Henson (*see* Henson et al. [2006] for details). The monthly average net surface heat flux was obtained from the National Centers for Environmental Prediction Global Ocean Data Assimilation System and downloaded from http://iridl.ldeo.columbia.edu.

the bloom is typically limited to a thin layer near the surface. As discussed by Stramska et al. (1995), blooms originating in deep mixed layers with abundant nutrients can lead to a much higher total biomass than could be supported in a thinner mixed layer. Garside and Garside (1993) proposed that up to half of the spring bloom primary production can occur before the onset of stratification. The early onset of blooms might, therefore, play an important role in the net carbon uptake, and will strongly influence the ecological dynamics later in the season.

Based on our findings, it may be possible to improve the representation of bloom dynamics in biogeochemical models by incorporating effects of finite turbulent mixing. Some models (Lévy et al. 1998) assume that phytoplankton are uniformly exposed to light within the mixed layer or the euphotic layer. This assumption is appropriate in the limit of a fully turbulent mixed layer as in Sverdrup (1953), but not when turbulence is weak and phytoplankton preferentially accumulate in regions with high net local growth. In the limit of weak mixing, the achieved growth rate of the phytoplankton population might be significantly underestimated by these models.

The critical surface heat flux, given in Eq. 19, is valid when the surface heat flux varies more slowly than the biological response. However, the surface heat flux also exhibits more rapid fluctuations in time, such as the diurnal cycle. Using additional numerical simulations (not shown) we found that a diurnal cycle with balanced heating and cooling does not generate enough vertical mixing to prevent a phytoplankton bloom, even if convection penetrates below the critical depth at night. However, when the cooling at night is stronger, and there is a net cooling of the surface each day, the resulting turbulence is sufficient to prevent a bloom. Based on these results, convective mixing generated by the diurnal cycle alone does not significantly affect the phytoplankton response to the mean forcing conditions. The heat flux used in the scaling expression in Eq. 19 should, therefore, be averaged for $\geq$ 1 d, but we have not explored how long the surface forcing needs to be weak in order for a bloom to develop.

In order to focus our attention on the influence of the role of turbulent convection on the timing of the spring bloom, we have made a number of simplifications. Nutrient limitation and grazing pressure were not explicitly included in our analysis of Eq. 2 or in the numerical simulations, but both of these will likely become important, particularly in the later stages of the bloom. We have also modeled the phytoplankton population using an Eulerian model instead of a particle-based Lagrangian approach. As a result, the instantaneous phytoplankton response depends only on the local light conditions. There is some evidence that in weak turbulence conditions, phytoplankton can adapt their physiology in response to their individual light conditions (Marra 1978; Lewis et al. 1984; Cullen and Lewis 1988).

In this paper, we have restricted our attention to mixing generated by turbulent convection. However, wind forcing can also strongly influence turbulence and stratification in the upper ocean. When wind-driven turbulence is sufficient to mix the phytoplankton concentration over a layer deeper than the critical depth, it could delay the onset of the spring bloom as estimated here based on the sign of the surface heat flux alone. The methodology developed in this paper, based on analytical theory and high-resolution numerical simulations, could be used to analyze the combined effects of convection and winds on the timing of the spring bloom. We intend to pursue this approach and derive a critical turbulence criterion that accounts for winds and buoyancy fluxes. Such a generalized criterion will be necessary to quantitatively test our hypothesis using additional field data.

Acknowledgments

We thank Michael Follows and Glenn Flierl for introducing us to the study of spring blooms. Jef Huisman, Ben Ward, Stephanie Dutkiewicz and an anonymous reviewer offered many valuable suggestions. This work was supported through ONR award N00014-08-1-1060. Ferrari acknowledges support from the Breene M. Kerr Professorship.

References

Behrenfeld, M. 2010. Abandoning Sverdrup's Critical Depth Hypothesis on phytoplankton blooms. Ecology **91:** 977–989, doi:10.1890/09-1207.1

Boss, E., and M. Behrenfeld. 2010. In situ evaluation of the initiation of the North Atlantic phytoplankton bloom. Geophys. Res. Lett. **37:** L18603, doi:10.1029/2010GL044174

Brainerd, K., and M. Gregg. 1995. Surface mixed and mixing layer depths. Deep-Sea Res. I **42:** 1521–1543, doi:10.1016/0967-0637(95)00068-H

Cullen, J., and M. Lewis. 1988. The kinetics of algal photoadaption in the context of vertical mixing. J. Plankton Res. **10:** 1039–1063, doi:10.1093/plankt/10.5.1039

Dale, F., and B. Heimdal. 1999. Seasonal development of phytoplankton at a high latitude oceanic site. Sarsia **84:** 419–435.

Deardorff, J. 1972. Numerical investigation of neutral and unstable planetary boundary layers. J. Atmos. Sci. **29:** 91–115, doi:10.1175/1520-0469(1972)029<0091:NIONAU>2.0.CO;2

———, and G. Willis. 1985. Further results from a laboratory model of the convective planetary boundary layer. Bound.-Layer Meteor. **32:** 205–236, doi:10.1007/BF00121880

Dutkiewicz, S., M. Follows, J. Marshall, and W. Gregg. 2001. Interannual variability of phytoplankton abundances in the North Atlantic. Deep-Sea Res. II **48:** 2323–2344, doi:10.1016/S0967-0645(00)00178-8

Ebert, U., M. Arrayas, N. Temme, B. Sommeijer, and J. Huisman. 2001. Critical conditions for phytoplankton blooms. Bull. Math. Biol. **63:** 1095–1124, doi:10.1006/bulm.2001.0261

Evans, G., and J. Parslow. 1985. A model of annual plankton cycles. Biol. Oceanogr. **3:** 327–347.

Fernando, H., R. Chen, and D. Boyer. 1991. Effects of rotation on convective turbulence. J. Fluid Mech. **228:** 513–547.

Follows, M., and S. Dutkiewicz. 2002. Meteorological modulation of the North Atlantic spring bloom. Deep-Sea Res. II **49:** 321–344, doi:10.1016/S0967-0645(01)00105-9

Garside, C., and J. Garside. 1993. The "f-ratio" on 20°W during the North Atlantic Bloom Experiment. Deep-Sea Res. II **40:** 75–90, doi:10.1016/0967-0645(93)90007-A

Ghosal, S., and S. Mandre. 2003. A simple model illustrating the role of turbulence on phytoplankton blooms. Bull. Math. Biol. **46:** 333–346.

Gran, H., and T. Braarud. 1935. A quantitative study on the phytoplankton of the Bay of Fundy and the Gulf of Maine (including observations on hydrography, chemistry and morbidity). J. Biol. Board Canada **1:** 219–467.

Gregg, M. 1991. The study of mixing in the ocean: A brief history. Oceanography **4:** 39–45.

Henson, S., J. Dunne, and J. Sarmiento. 2009. Decadal variability in North Atlantic phytoplankton blooms. J. Geophys. Res. **114:** C04013, doi:10.1029/2008JC005139

———, I. Robinson, J. Allen, and J. Waniek. 2006. Effect of meteorological conditions on interannual variability in timing and magnitude of the spring bloom in the Irminger Basin, North Atlantic. Deep-Sea Res. I **53:** 1601–1615, doi:10.1016/j.dsr.2006.07.009

Huisman, J., M. Arrayás, U. Ebert, and B. Sommeijer. 2002. How do sinking phytoplankton species manage to persist? Am. Nat. **159:** 245–254, doi:10.1086/338511

———, J. Sharples, J. Stroom, P. Visser, W. Kardinaal, J. Verspagen, and B. Sommeijer. 2004. Changes in turbulent mixing shift competition for light between phytoplankton species. Ecology **85:** 2960–2970, doi:10.1890/03-0763

———, P. van Oostveen, and F. Weissing. 1999. Critical depth and critical turbulence: Two different mechanisms for the development of phytoplankton blooms. Limnol. Oceanogr. **44:** 1781–1787, doi:10.4319/lo.1999.44.7.1781

Jamart, B., D. Winter, K. Banse, G. Anderson, and R. Lam. 1977. A theoretical study of phytoplankton growth and nutrient distribution in the Pacific Ocean off the northwestern U.S. coast. Deep-Sea Res. **24:** 753–773.

Klinger, B., J. Marshall, and U. Send. 1996. Representation of convective plumes by vertical adjustment. J. Geophys. Res.-Oceans **101:** 18175–18182, doi:10.1029/96JC00861

Levy, M., and H. Fernando. 2002. Turbulent thermal convection in a rotating stratified fluid. J. Fluid Mech. **467:** 19–40, doi:10.1017/S0022112002001350

Lévy, M., L. Mémery, and G. Madec. 1998. The onset of a bloom after deep winter convection in the northwestern Mediterranean Sea: Mesoscale process study with a primitive equation model. J. Mar. Syst. **16:** 7–21doi: 10.1016/S0924-7963(97)00097-3

Lewis, M., E. Horne, J. Cullen, N. Oakey, and T. Platt. 1984. Turbulent motions may control phytoplankton photosynthesis in the upper ocean. Nature **311:** 49–50, doi:10.1038/311049a0

Marra, J. 1978. Phytoplankton photosynthetic response to vertical movement in a mixed layer. Mar. Biol. **46:** 203–208, doi:10.1007/BF00390681

Miller, C. 2004. Biological oceanography. Blackwell.

Molemaker, M., and H. Dijkstra. 1997. The formation and evolution of a diffusive interface. J. Fluid Mech. **331:** 199–229, doi:10.1017/S0022112096003862

Peeters, F., D. Straile, A. Lorke, and D. Ollinger. 2007. Turbulent mixing and phytoplankton spring bloom development in a deep lake. Limnol. Oceanogr. **52:** 286–298, doi:10.4319/lo.2007.52.1.0286

Riley, G. 1946. Factors controlling phytoplankton populations on Georges Bank. J. Mar. Res. **6:** 54–72.

Send, U., and J. Marshall. 1995. Integral effects of deep convection. J. Phys. Oceanogr. **25:** 855–872, doi:10.1175/1520-0485(1995)025<0855:IEODC>2.0.CO;2

Smetacek, V., K. Bröckel, B. Zeitzschel, and W. Zenk. 1978. Sedimentation of particulate matter during a phytoplankton spring bloom in relation to the hydrographical regime. Mar. Biol. **47:** 211–226, doi:10.1007/BF00541000

Stramska, M., T. Dickey, A. Plueddemann, and R. Weller. 1995. Bio-optical variability associated with phytoplankton dynamics in the North Atlantic Ocean during spring and summer of 1991. J. Geophys. Res. **100:** 6621–6632, doi:10.1029/94JC01447

Sverdrup, H. 1953. On conditions for the vernal blooming of phytoplankton. Journal du Conseil International pour l'Exploration de la Mer **18:** 287–295.

Taylor, J. 2008. Numerical Simulations of the Stratified Oceanic Bottom Boundary Layer. Ph.D. thesis, University of California, San Diego.

———, and R. Ferrari. 2010. Buoyancy and wind-driven convection at mixed-layer density fronts. J. Phys. Oceanogr. **40:** 1222–1242, doi:10.1175/2010JPO4365.1

Thorpe, S. 2005. The turbulent ocean. Cambridge Univ. Press, Cambridge.

Townsend, D., L. Cammen, P. Holligan, D. Campbell, and N. Pettigrew. 1994. Causes and consequences of variability in the timing of spring phytoplankton blooms. Deep-Sea Res. I **41:** 747–765, doi:10.1016/0967-0637(94)90075-2

———, M. Keller, M. Sieracki, and S. Anderson. 1992. Spring phytoplankton blooms in the absence of vertical water column stratification. Nature **360:** 59–62, doi:10.1038/360059a0

Waniek, J. 2003. The role of physical forcing in initiation of spring blooms in the northeast Atlantic. J. Mar. Syst. **39:** 57–82, doi:10.1016/S0924-7963(02)00248-8

Associate editor: Craig L. Stevens

Received: 16 February 2011
Accepted: 05 July 2011
Amended: 16 July 2011